ISSN 0003-701X, Applied Solar Energy, 2024, Vol. 60, No. 1, pp. 49–57. © Allerton Press, Inc., 2024.

SOLAR ENERGY CONCENTRATORS

Experimental Study on the Optimization of Thermal Performance in a Solar Steam Generator

Hongjun Wang[a, b], Qiangqiang Zhang[a, b, *], Xin Li[a, b, **], Xia Zhang[c], Tianzeng Ma[a], Haoyang Yin[a, b], and Khurshida F. Sayfieva[d]

[a] *Institute of Electrical Engineering, Chinese Academy of Sciences, Beijing, 100190 China*
[b] *University of Chinese Academy of Sciences, Beijing, 100049 China*
[c] *Taian Institute of Quality and Technology Inspection, Tai'an City, Shandong Province, 217000 China*
[d] *Tashkent State Technical University, Tashkent, 100095 Uzbekistan*
** e-mail: zhangqiangqiang@mail.iee.ac.cn*
*** e-mail: drlixin@mail.iee.ac.cn*

Received November 14, 2023; revised January 17, 2024; accepted February 3, 2024

Abstract—SOEC (Solid Oxide Electrolysis Cell) require high temperature steam, but generating steam with electricity is very energy intensive. Concentrated solar power can be a good substitute for electricity to generate high temperature steam. In this paper, the thermal performance of a solar steam generator is researched. The steam generator improves the heat transfer capacity by installing porous ceramic material inside and using spray cooling technique. Due to the limited heat transfer capacity of previous steam generators, other types of steam generators can only produce steam with a temperature below 700°C. The steam generator in this paper has a high thermal efficiency depending on the nozzle characteristics. Therefore, the steam generator has obvious advantages in terms of generating high-temperature steam. The experimental results show that the instantaneous thermal efficiency of the steam generator with a new nozzle can reach a maximum of 58% when the solar irradiation power is 2.26 kW and the inlet water flow rate is 1.23 kg/h. At this time, the steam generator can produce high temperature water vapour at a maximum temperature of 715.4°C. The optimized solar steam generator was also coupled with the SOEC system, and hydrogen production was successfully achieved by experimental means. The solar SOEC system has great potential for hydrogen production.

Keywords: steam generator, irradiation power, nozzle characteristics, thermal efficiency, hydrogen production
DOI: 10.3103/S0003701X23601692

INTRODUCTION

Among the many current hydrogen production methods, electrolysis of water is a technology with significant development prospects and is capable of being applied on a large scale [1–3]. Compared with other types of electrolysis for hydrogen production (e.g., proton exchange membrane electrolysis) [4–6], hydrogen production by solid oxide electrolysis cell (SOEC) can reduce the polarization overpotential, accelerate the reaction rate of electrodes, reduce the electrical energy consumption, and improve the energy conversion efficiency of the system [7].

Conventional SOEC requires a large amount of electrical energy to meet the energy needs of the electrolysis process [8–10], which includes the electrical energy required for the electrolysis reaction, the electrical heating to provide the SOEC system with the high-temperature gas source required for electrolysis, and to maintain the SOEC in a high-temperature environment. Using solar energy to provide the SOEC with high-temperature steam for electrolysis the consumption of electric energy in this system can be reduced [11]. The energy conversion efficiency of the system can thus be further improved.

SOEC usually operates at high temperatures of 700–1000°C [12], a solar high-temperature steam generator with good heat transfer performance, and that can continuously generate stable high-temperature steam at these temperatures [13], plays an important role in the SOEC coupled with solar system. Therefore, the current studies related to solar steam generator are as follows.

Ben-Zvi et al. proposed a new solar tube steam generator by dividing the position of the heat pipe on the steam generator into an evaporation part and a superheated part. Using simulations, the results showed that the generator can produce superheated steam at 550°C and 150 bars [14]. Houaijia et al. designed a solar tube heat absorber that can produce high-temperature steam at 700°C, which can be used

for electrolysis at high temperatures [15]. Liu et al. proposed a glass tube-type solar steam generator, and proved through experiments that it could generate steam with a temperature of up to 200°C at a pressure of 0.55 MPa. It could produce stable, saturated steam with a temperature higher than 150°C and a thermal efficiency above 30% in the range of pressure of 0.1 to 0.55 MPa [16]. Pye et al. proposed a novel solar tube steam generator and, through experiments, the results showed that it can produce superheated steam at 560°C when the DNI is 1052 W/m^2 [17]. The results of experiments by Swanepoel et al. on a steam generator showed that when the total incident area of the heat absorber was 2.7 m^2 and the rate of flow of water was 0.294 g/s, the fluid gained 861 W of heat, while the temperature at the outlet was 343°C under an intensity of solar radiation of 757 W/m^2. This yielded a thermal efficiency of the heat absorber of 42% [18]. Indira et al. designed and built a hybrid system for using photovoltaic/thermal solar energy, and validated its model through simulations and tested its experimental performance [19]. The results showed that its maximum electrical efficiency was 4.86% and maximum thermal efficiency was 40% when the intensity of solar radiation was higher than 1000 W/m^2. Zhang et al. developed a solar steam generator through theoretical modeling, and the results showed that the spray had an important influence on radiation-induced conduction in the generator [20]. Wang et al. proposed a novel solar steam generator to improve the heat exchange capacity of the steam generator by installing a porous structure and spray cooling inside the generator. The experimental results show that this solar steam generator can produce high-temperature steam at 800°C using concentrated solar energy [21].

Although [21] proposes a novel solar steam generator and uses concentrated solar energy to generate high-temperature steam at 800°C, the solar steam generator in [21] has a low thermal efficiency (the maximum thermal efficiency of the steam generator does not exceed 31% when generating high-temperature water vapor above 700°C). In this paper, based on the research of [21], the nozzle in the solar steam generator of [21] is optimized to further improve the corresponding atomization performance of the nozzle. Compared with [21], the optimized solar steam generator in this paper can not only produce high-temperature water vapor in the same temperature range as that of [21], but also the thermal efficiency can be greatly improved. Therefore, the high thermal efficiency of the steam generator in this paper has a clear advantage in light–heat conversion capacity. The optimized solar steam generator was also coupled with the SOEC system, and hydrogen production was successfully achieved by experimental means. This study can lay the corresponding foundation for the future application of solar SOEC systems for photothermal synergistic hydrogen production in real environments.

EXPERIMENTAL DETAILS

The solar steam generator in this paper is optimized compared to [21]. Solar energy is converted into thermal energy in the generator, then the supercooled water is passed through the heat absorber in the generator, producing high-temperature superheated water vapor. A diagram and photographs of the high-temperature steam generation platform are shown in Figs. 1 and 2. The experimental schemes of this solar steam generator can be found in [21].

The solar steam generator consists of a porous ceramic heat absorber, an insulated shell, quartz glass, a high-pressure spray system, and a support structure. The porous ceramic heat-absorbing body is a silicon carbide cylinder with a diameter of 80 mm. The porous silicon carbide ceramic material has a porosity of 70%, a pore diameter of 15 PPI, and a thickness of 50 mm, and is mounted in the center cavity of the generator. The quartz glass, with a diameter of 115 mm and a thickness of 15 mm, is mounted at the front of the generator. The insulated enclosure consists of refractory bricks and insulating cotton, which is designed to minimize the heat conduction losses from the generator to the outside during the experiment. The high-pressure spraying system consists of submersible pump, high-pressure spraying machine, and atomizing nozzle, in which the nozzle diameter is 0.1–0.2 mm. The deionized water for the experiment was passed through a submersible pump and then a high-pressure sprayer and atomized to form small droplets under the action of nozzles [21].

The high-temperature steam produced by the solar steam generator is passed into the SOEC stack, where an electrolysis reaction occurs to produce hydrogen. The SOEC stack used in this paper is made of SOFCMAN-A-SCS2000 module manufactured by SOFCMAN, which consists of an anode supporting 30 single Ni-YSZ/YSZ/CGO/LSCF-CGO cells, SUS430 metal connectors, and sealing materials [22]. The dimensions of the stack are 190 × 190 × 440 mm, and the effective electrolytic area of a single cell is 150 cm^2. The gas path of the stack is fully closed on the cathode side and semi-open on the anode side, and the oxygen generated from the anode is discharged to the atmosphere from the semi-open structure of the stack during the reaction process, as shown in Fig. 3. Specific information for the measuring instruments is shown in Table 1.

The diameter of the atomizing nozzle ranges from 0.1 to 0.2 mm, making it one of the core components

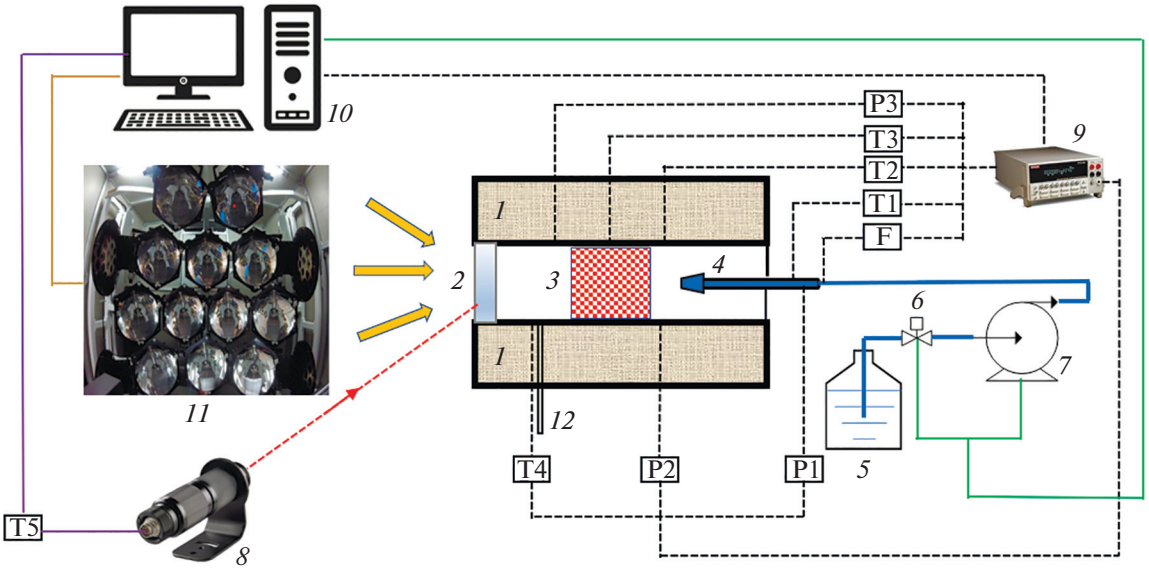

Fig. 1. Diagram of the platform for high-temperature steam generation [21]: (*1*) insulated shell; (*2*) quartz glass; (*3*) porous silicon carbide ceramic; (*4*) micronozzle; (*5*) water tank; (*6*) regulating valve; (*7*) high-pressure pump; (*8*) infrared temperature-measuring instrument; (*9*) local display equipment; (*10*) computer for data acquisition; (*11*) solar simulator; (*12*) steam outlet.

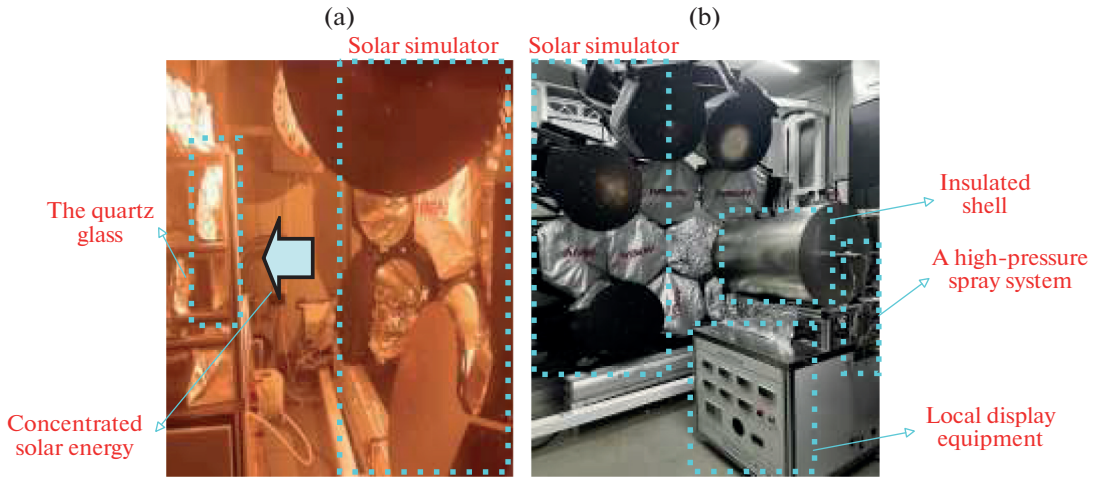

Fig. 2. Photographs of high-temperature steam generation platform [21]: (a) Photograph of the experiment with the solar simulator turned on. (b) Photograph of the overall experimental system.

Table 1. Specific information for the measuring instruments [22]

Name	Quantity	Specification	Accuracy
Thermocouple (steam generator)	4	Type K	±0.1%
Pressure sensor (steam generator)	3	Model PS6000-CR-BZ-A1-B-2/D	±0.25%
Infrared Thermometer	1	T40-LT-70-SF2-2	±1.0%
Thermocouple (SOEC)	3	Type K	±0.0075t (t-Temperature of thermocouple, °C)
Pressure sensor (SOEC)	2	Model MN100-G5M14AI600KPaF	0.5%
Flowmeter (H_2)	1	D07-19B	0.2%
Flowmeter (AIR)	1	Model D07-19BM	1.05%

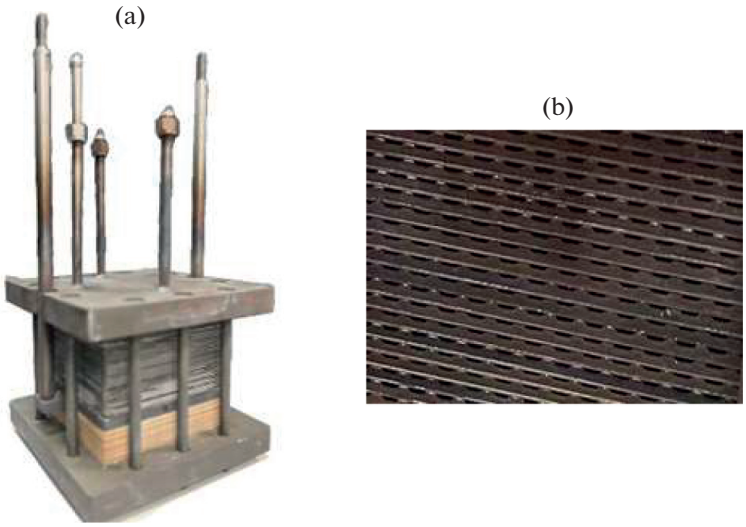

Fig. 3. SOEC stack: Photographs of the (a) SOEC stack and (b) anode side outlet [22].

of the solar steam generator. It consists of the nozzle head and connecting base, as illustrated in Fig. 4. The schematic shows that maintaining a good sealing performance is critical when utilizing the nozzle in a high-temperature environment. In this regard, the connection points between the nozzle and the connection base, as well as the connection base and the water inlet port play a critical role. According to a report by [21], the sealing performance is ensured by welding all of the above parts, as shown in Fig. 5a.

This nozzle, with a good sealing performance, was tested at room temperature and pressure with the inlet flow rate set to 3.96 L/h at an inlet pressure of 0.3 MPa. The flow rate of the nozzle was compared with that of the B3 model nozzle from CSAN FOG Nozzle INC (Tianjin, China) at the same inlet pressure, as shown in Fig. 6. It can be seen that the inlet pressure increases, the inlet flow rate of the B3 model nozzle increases. When the inlet pressure increases from 0.3 to 7 MPa, the inlet flow rate of the B3 model nozzle increases from 1.2 to 6.22 L/h. And at an inlet pressure of 0.3 MPa, the inlet flow rate of [21] is 3.96 L/h. The inlet flow rate, as reported by [21], is higher at the same inlet pressure, and the atomization performance of the nozzle is poorer compared to that of the B3 model nozzle from CSAN FOG Nozzle INC (Tianjin, China). After switching the solar simulator on, the heat transfer process atomizes the supercooled water through the nozzle. This leads to the formation of small droplets that are sprayed onto a porous silicon carbide ceramic material and eventually form high-temperature steam. The solar steam generator reported in [21] produces high-temperature water vapor. Additionally, owing to the poor atomization performance of the nozzle, the steam generator has a low thermal efficiency of up to 31% when generating high-temperature water vapor above 700°C. Therefore, in this study, structural optimization was performed for the nozzle used in the solar steam generator reported previously. To seal the nozzle, the distance between the nozzle and the base was maximized, as shown in Fig. 5b. This was done to prevent any dam-

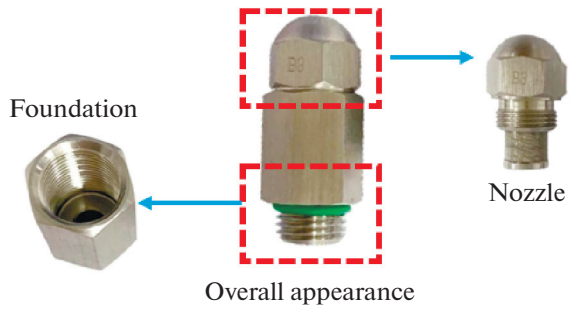

Fig. 4. Diagram of the nozzle structure.

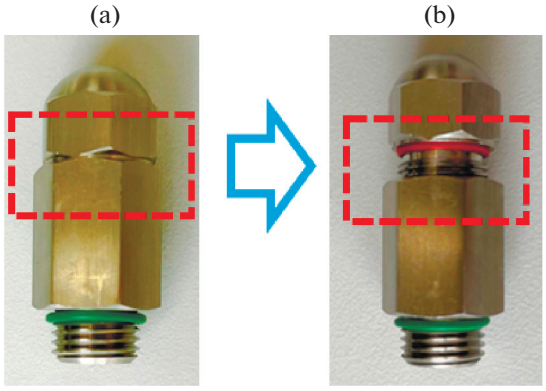

Fig. 5. (a) Nozzle in [21]. (b) Optimized nozzle.

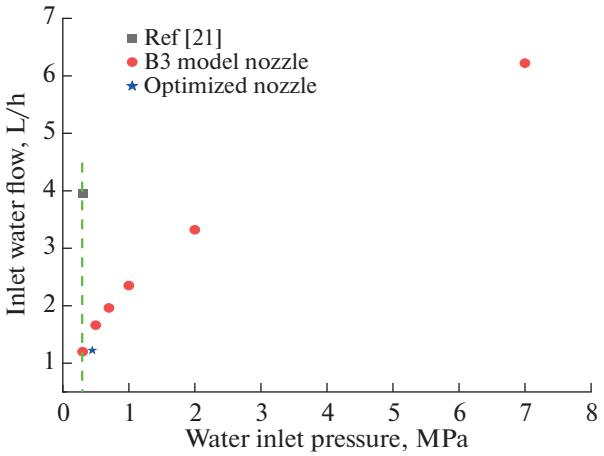

Fig. 6. Variations in inlet pressure and water flow.

age to the nozzle structure caused by the high temperature generated during the welding process when the nozzle is connected to the base, thus affecting the spray performance of the nozzle. When the nozzle operates under a differential pressure of 0.44 MPa, the optimized nozzle inlet flow rate measures 1.23 L/h. At this flow rate, the nozzle flow rate closely aligns with that of the corresponding nozzle under the differential pressure in the B3 model nozzle, as shown in Fig. 6. Consequently, it can be inferred that the spray performance of the optimized nozzle is more consistent with that of the B3 model nozzle and achieves a superior atomization effect.

RESULTS AND DISCUSSION

The solar steam generator in this paper is used with optimized nozzles for the following experiments. When the solar simulator is switched on, Figs. 7a and 7b show the pressure and inlet water temperature of the solar steam generator against time during the heat exchange process. It can be seen from Fig. 7 that the pressure before and after the nozzle, and the inlet water temperature of the steam generator, fluctuate to a lesser extent as the heat exchange process proceeds. When the irradiation power is 2.26 kW and the differential pressure of the nozzle is 0.44 MPa, the inlet water temperature of the steam generator is kept at about 30°C. When the differential pressure of the nozzle remains unchanged, it is considered that the inlet water flow rate of the steam generator remains unchanged, and the inlet water flow rate through the electronic scale to measure changes in water weight over a period of time is 1.23 kg/h.

Figure 8 shows the variation of the front-end pressure of the steam generator with time during the heat transfer process when the solar irradiation power is constant. From Fig. 8, it can be seen that the front-end pressure of the steam generator remains around 0.037 MPa when the irradiation power is 2.26 kW and the inlet water flow rate is 1.23 kg/h.

The difference in enthalpy between the inlet and outlet of water Δh is:

$$\Delta h = h_{\text{out}} - h_{\text{in}}. \quad (1)$$

Then, the thermal efficiency of the steam generator η is:

$$\eta = \frac{\int_{t_0}^{t_0+\Delta t} \dot{m}\Delta h dt}{\int_{t_0}^{t_0+\Delta t} Q dt}, \quad (2)$$

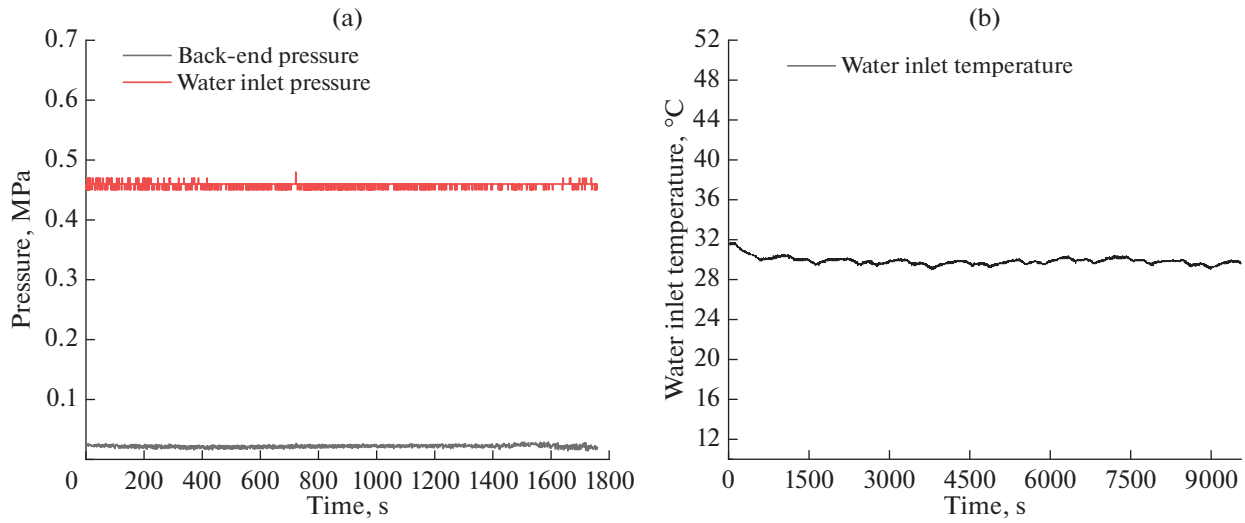

Fig. 7. The steam generator: (a) Pressure variations in the nozzle. (b) Inlet temperature variations in the steam generator.

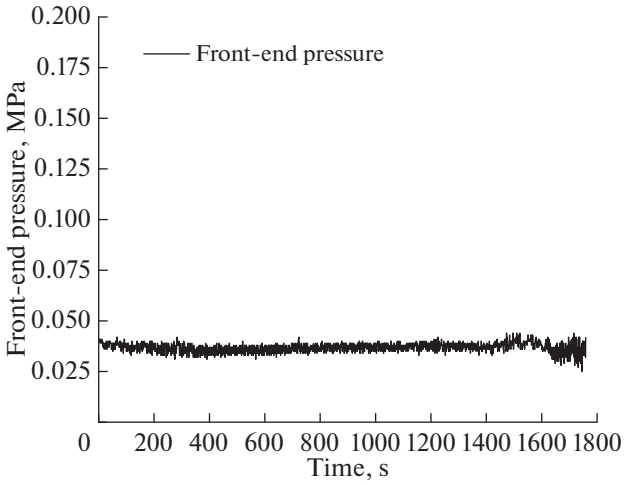

Fig. 8. Variations in the front-end pressure of the steam generator.

where h_{in} is the enthalpy of water at the inlet (kJ/kg), h_{out} is that at the outlet (kJ/kg), Q is the solar irradiation of the simulator (kW), $\dot{m}$ is the mass flow of water (kg/s).

Figures 9a and 9b show the variation of thermal performance using the steam generator from [21] and the optimized steam generator. Figure 9a shows the variation of outlet temperature with time during the heat exchange process using the steam generator from [21] and the optimized steam generator. It can be seen that when the solar simulator is turned on and the radiation power is 6.07 kW in [21] and 2.26 kW in this paper, both solar steam generators are able to produce high-temperature superheated water vapor within a given temperature range (690–720°C), and the peak outlet temperature can be more than 800°C in the multi-operating condition test [21]. According to [21], this new type of solar steam generator offers a significant advantage in producing high-temperature vapor because of the installation of a porous structure inside the generator and the spray cooling method used. Figure 9b shows the variation of thermal efficiency during the relatively stable phase using the steam generator from [21] and the optimized steam generator. When the solar simulator is turned on and the radiation power is 6.07 kW in [21] and 2.26 kW in this paper, the thermal efficiency of the steam generator from [21] is up to 30.7%; the optimized steam generator is up to 58%, and the difference in thermal efficiency between the two solar steam generators can be up to 27.3%. This is due to the nozzle used in the spray cooling in [21]. The spray characteristics of the nozzle deterioration, resulting in water and generator of porous silicon carbide ceramic heat absorber heat transfer performance between the deterioration of the water, in order to make the water vapor maintain at a temperature of 700°C or higher, for the solar steam generator in [21], it is necessary to increase more irradiation power. The heat absorption of the porous silicon carbide ceramic material is increased, so that the heat exchange between the water and the porous silicon carbide ceramic material is increased, and the final temperature of the water vapor is increased. According to Eq. (2), when the heat absorption is constant, the higher the irradiation power, the higher the temperature of the water vapor produced, and the lower the thermal efficiency of the steam generator. For the optimized solar steam generator in this paper, less irradiation power is invested to produce high-temperature water vapor in the same temperature range when compared to the generator in [21]. According to Eq. (2), the thermal efficiency of the steam generator increases with decreasing irradiation power input at constant heat absorption. The solar steam generator in this paper has a high thermal efficiency and therefore has a significant advantage in terms of photothermal conversion performance.

The optimized solar steam generator is coupled with the SOEC system. The generated high-temperature water vapor is passed into the SOEC stack at an operating temperature of 730°C, where an electrolysis reaction occurs and ultimately hydrogen is produced.

According to the Nernst equation, the equilibrium voltage of the SOEC can be expressed as:

$$E = E_0 + \frac{RT}{2F}\ln\left[\frac{P_{H_2}\left(P_{O_2}\right)^{0.5}}{P_{H_2O}}\right], \quad (3)$$

where R is the gas constant (J/mol), T is the electrolysis temperature (K), P_{H_2}, P_{O_2}, P_{H_2O} indicate the partial pressures of hydrogen, oxygen, and water vapor, respectively. E_0 is the standard electric potential, E_0 is related to the electrolysis temperature.

The electrolytic performances of the system during electrolysis of SOEC stack is shown in Figs. 10a and 10b. Figure 10a indicates that the electrolytic current increases from 76.6 to 102.5 A when the electrolytic voltage is increased from 39.7 to 43.7 V. The electrolytic power increases from 3042.8 to 4482.3 W when the electrolytic voltage is increased from 39.7 to 43.7 V (Fig. 10b). The electrolytic voltage of SOEC comprises the equilibrium voltage during electrolysis and total overpotential. According to the Nernst equation, the equilibrium voltage is determined by the electrolysis temperature and the partial pressures of the reactants on both the cathode and anode sides of the components. The equilibrium voltage of the SOEC remains constant when the conditions on both the cathode and anode sides (temperature and partial pressure) are kept constant. The total overpotential of

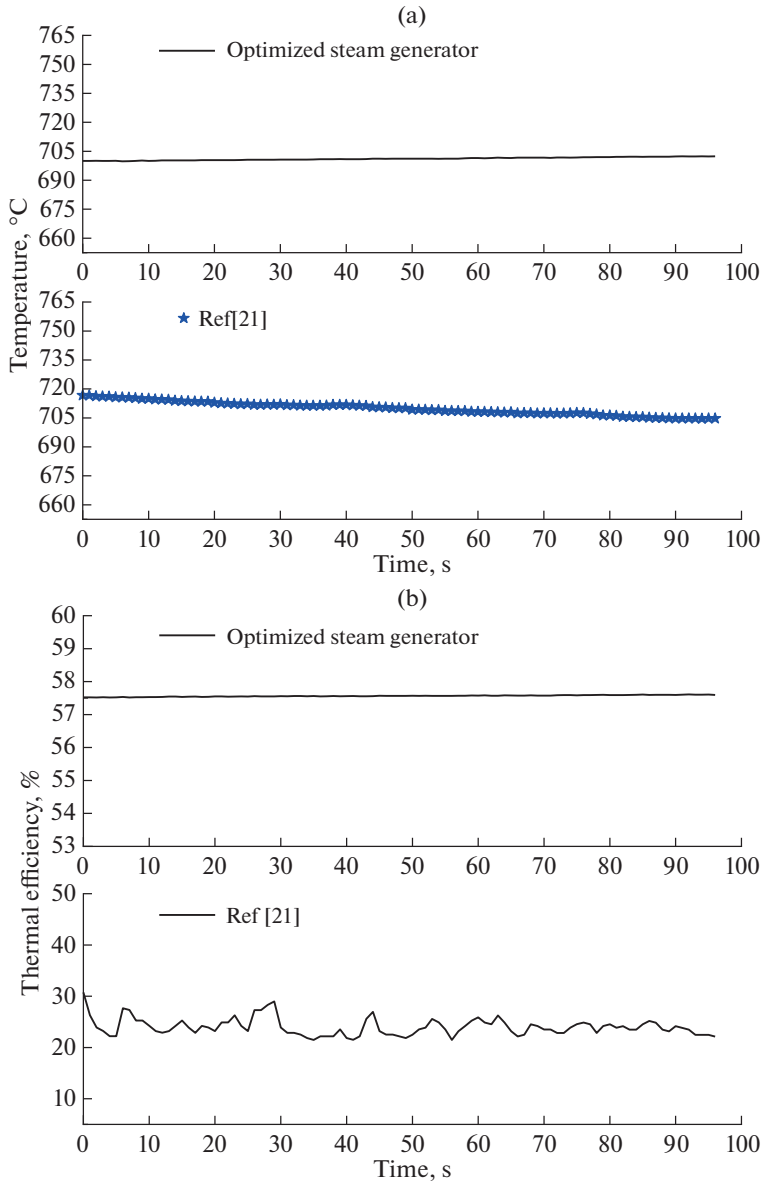

Fig. 9. Comparison of thermal performance between [21] and the optimized steam generator. Variations in (a) temperature and (b) thermal efficiency.

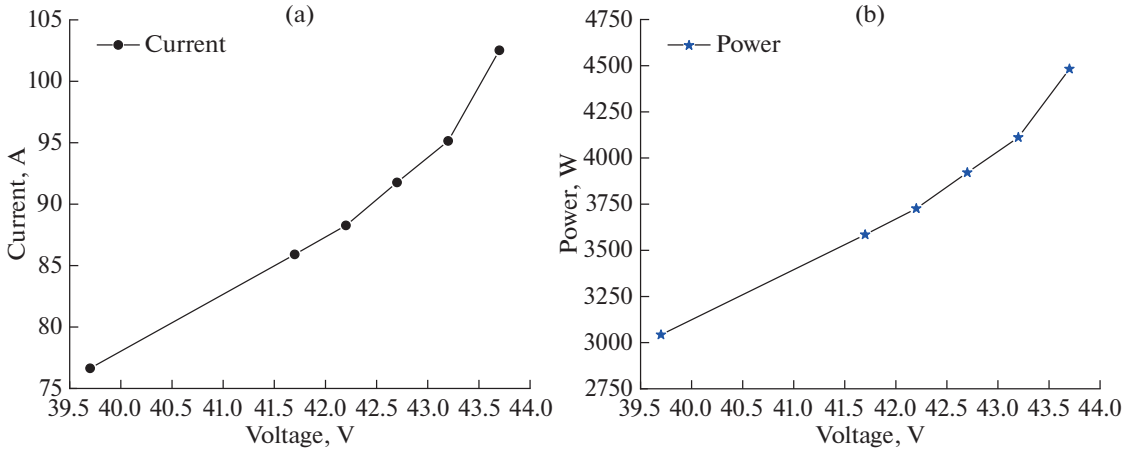

Fig. 10. Electrolytic performances of the system. Variations in (a) voltage-current and (b) voltage-power.

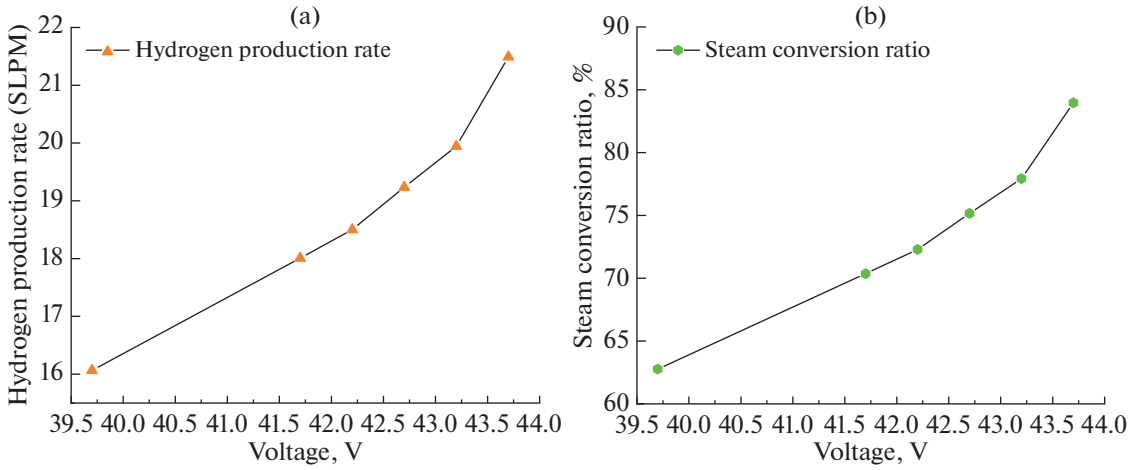

Fig. 11. Performance of the hydrogen production of the system. (a) Hydrogen production rate. (b) Steam conversion ratio.

SOEC is comprised of three components: ohmic, activation, and concentration overpotentials. All three of these overpotentials exhibit a certain positive correlation with the current density. When the equilibrium voltage is maintained at a constant value, and the electrolytic voltage is gradually increased, the total overpotential of the SOEC gradually increases, leading to a corresponding increase in the electrolytic current. As the total overpotential increases, the corresponding polarization loss increases and the final electrolytic power required gradually increases.

The hydrogen production performance of the system during SOEC stack electrolysis is shown in Fig. 11a and 11b. Figure 11a shows that the hydrogen production rate of the system increases from 16 to 21.5 SLPM as the electrolysis voltage is increased from 39.7 to 43.7 V. When the electrolysis voltage is gradually increased, the corresponding electrolysis current gradually increases in accordance with Faraday's law of current, resulting in more hydrogen production. As shown in Fig. 11b, the steam conversion ratio of the system increases from 62.8 to 84% as the electrolysis voltage is increased from 39.7 to 43.7 V. With the increasing voltage, the electrolysis current also increases gradually, leading to a greater consumption of water vapor in the electrolysis reaction. Consequently, when the incoming water flow rate remains constant, the steam conversion ratio of the system becomes progressively higher.

CONCLUSIONS

In this study, building upon the findings of [21], the optimization of the nozzle in the solar steam generator was performed to improve its atomization performance. The optimized solar steam generator was then coupled with the SOEC system, and through experimental methods, hydrogen was successfully produced. Consequently, the following conclusions were drawn:

In comparison to the results presented in [21], the optimized solar steam generator in this study demonstrates the capability to generate high-temperature water vapor at 715.4°C when exposed to a solar irradiation power of 2.26 kW and an inlet water flow rate of 1.23 kg/h. Furthermore, the thermal efficiency of the steam generator can reach a maximum of 58% in the relatively stable stage. The high thermal efficiency of the steam generator has a clear advantage in terms of light-to-heat conversion capacity. The production of high-temperature water vapor by the steam generator lays the corresponding foundation for subsequent photothermal synergistic hydrogen production in the solar SOEC system. When the solar irradiation power is 2.26 kW, with an inlet water flow rate of 1.23 kg/h, and the system operating at a temperature of 730°C while performing electrolysis at a constant voltage, the solar SOEC system can produce hydrogen at a rate of up to 21.5 SLPM. Additionally, the water vapor conversion rate can reach up to 84%.

ACKNOWLEDGMENTS

The research is supported by schools and professors.

FUNDING

This work was supported by the Beijing Natural Science Foundation (no. 3222049) and the National Natural Science Foundation of China (no. 52176209). This research was also funded by International Partnership Program of Chinese Academy of Sciences (182111KYSB20200021). The authors thank the Institute of Electrical Engineering, CAS (E155710101) for financial support.

CONFLICT OF INTEREST

The authors of this work declare that they have no conflicts of interest.

REFERENCES

1. Grube, T., et al., A techno-economic perspective on solar-to-hydrogen concepts through 2025, *Sustainable Energy Fuels,* 2020, vol. 4.
2. Otto, A., Robinius, M., Grube, T., Schiebahn, S., and Stolten, D., Power-to-steel: Reducing CO_2 through the integration of renewable energy and hydrogen into the German steel industry, *Energies,* 2017, vol. 10, no. 4, p. 451.
3. Allaev, K.R. and Avezova, N.R., Hydrogen—the future of power engineering for the world and Uzbekistan, *Appl. Sol. Energy,* 2022, vol. 57, no. 6, pp. 575–583.
4. Ebbesen, S.D., Jensen, S.H., Hauch, A., and Mogensen, M.B., High temperature electrolysis in alkaline cells, solid proton conducting cells, and solid oxide cells, *Chem. Rev.,* 2014, vol. 114, no. 21, pp. 10697–10734.
5. Hauch, A., et al., Recent advances in solid oxide cell technology for electrolysis, *Science,* 2020, vol. 370, no. 6513, p. 186.
6. Lahoussine Ouali, H.A., Moussaoui, M.A., and Mezrhab, A., Hydrogen production from two commercial Dish/Stirling systems compared to the photovoltaic system—case study: Eastern Morocco, *Appl. Sol. Energy,* 2021, vol. 56, no. 6, pp. 466–476.
7. Jang, D., Kim, J., Kim, D., Han, W.-B., and Kang, S., Techno-economic analysis and Monte Carlo simulation of green hydrogen production technology through various water electrolysis technologies, *Energy Convers. Manage.,* 2022, vol. 258.
8. Li, Q., Zheng, Y., Guan, W., Jin, L., Xu, C., and Wang, W.G., Achieving high-efficiency hydrogen production using planar solid-oxide electrolysis stacks, *Int. J. Hydrogen Energy,* 2014, vol. 39, no. 21, pp. 10833–10842.
9. Ni, M., Leung, M.K.H., and Leung, D.C., Energy and exergy analysis of hydrogen production by solid oxide steam electrolyzer plant, *Int. J. Hydrogen Energy,* 2007, vol. 32, no. 18, pp. 4648–4660.
10. Wang, Z., Mori, M., and Araki, T., Steam electrolysis performance of intermediate-temperature solid oxide electrolysis cell and efficiency of hydrogen production system at 300 Nm3h-1, *Int. J. Hydrogen Energy,* 2010, vol. 35, no. 10, pp. 4451–4458.
11. Avezova, N.R., Rakhimov, E.Y., Khaitmukhamedov, A.E., Boliev, B.B., and Usmonov, A.Y., Dependence of techno-economic and ecological indicators of flat-plate solar water heating collectors in hot water supply systems from the temperature of heating water, *Appl. Sol. Energy,* 2018, vol. 54, no. 4, pp. 297–301.
12. Schiller, G., et al., Solar heat integrated solid oxide steam electrolysis for highly efficient hydrogen production, *J. Power Sources,* 2019, vol. 416, pp. 72–78.
13. Niyazov, S.K., Kasimov, F.S., Vokhidov, A.U., and Abduxamidov, D.U., Thermal engineering and technical-economical indicators of seasonal flat-plate capacitive solar water-heating collectors, *Appl. Sol. Energy,* 2023, vol. 59, no. 3, pp. 239–243.
14. Ben-Zvi, R., Epstein, M., and Segal, A., Simulation of an integrated steam generator for solar tower, *Sol. Energy,* 2012, vol. 86, no. 1, pp. 578–592.
15. Houaijia, A., et al., Solar hydrogen by high-temperature electrolysis: Flowsheeting and experimental analysis of a tube-type receiver concept for superheated steam production, *Energy Procedia,* 2014, vol. 49, no. 49, pp. 1960–1969.
16. Liu, Z., Tao, G., Lu, L., and Wang, Q., A novel all-glass evacuated tubular solar steam generator with simplified CPC, *Energy Convers. Manage.,* 2014, vol. 86, pp. 175–185.
17. Pye, J., Coventry, J., Venn, F., Zapata, J., and Logie, W., Experimental testing of a high-flux cavity receiver, in *SolarPACES 2016,* 2016.
18. Swanepoel, J.K., le Roux, W.G., Lexmond, A.S., and Meyer, J.P., Helically coiled solar cavity receiver for micro-scale direct steam generation, *Appl. Therm. Eng.,* 2021, vol. 185, p. 116427.
19. Sripadmanabhan Indira, S., Aravind Vaithilingam, C., Sivasubramanian, R., Chong, K.-K., Narasingamurthi, K., and Saidur, R., Prototype of a novel hybrid concentrator photovoltaic/thermal and solar thermoelectric generator system for outdoor study, *Renewable Energy,* 2022, vol. 201, pp. 224–239.
20. Zhang, Q. and Li, X., The effect of spray on the radiation transfer of concentrated solar irradiation in a novel designed solar steam generator, *Renewable Energy,* 2023, vol. 206, pp. 13–23.
21. Wang, H., Zhang, Q., Li, X., Zhang, X., and Ma, T., Experimental investigation into the thermal performance of a solar steam generator based on spray cooling heat transfer and porous silicon carbide ceramic, *J. Renewable Sustainable Energy,* 2023, vol. 15, no. 5.
22. Wang, H., Zhang, Q., Li, X., Ma, T., and Sayfieva, K.F., Investigation into the hydrogen production performance of a novel 5-kW hybrid-system composed of a solar steam generator directly connected with conventional solid oxide electrolysis cells, *Energy Convers. Manage.,* 2024, vol. 301, p. 118023.